GNSS-aided INS Integrity Concept

O. García Crespillo, A. Grosch, B. Belabbas, and M. Rippl
German Aerospace Center (DLR), Germany

BIOGRAPHY

Omar García Crespillo holds a diploma in Telecommunication Engineering from the University of Málaga in Spain. He made his final diploma thesis at the Institute of Communication and Navigation of the German Aerospace Center (DLR) on the topic of multi-sensor railway navigation in 2012. In 2013, he joined the Navigation department of DLR where his current field of research includes multi-sensor fusion algorithms for integrity based GNSS/INS navigation.

Anja Grosch received the German diploma in Computer Engineering from the Ilmenau University of Technology, Germany in 2007. After her graduation, she continued working for the communications department in the area of channel coding, OFDM systems and relay networks. Since March 2008, she has joined the DLR's Institute of Communications and Navigation. Her main focus has been multi-sensor fusion algorithms, especially GNSS and INS integrated systems, and the development of corresponding integrity concepts optimized for different safety-of-life applications such as civil aviation and railway.

Boubeker Belabbas is the leader of the Navigation Integrity Group of the Institute of Communications and Navigation at the German Aerospace Center (DLR) in Oberpfaffenhofen near Munich. He obtained a Master of Science degree in Mechanical Engineering from École Nationale Supérieure de l'Electricité de Mécanique in Nancy (France) and a specialized Master in Aerospace Mechanics from École Nationale Supérieure de l'Aeronautique et de l'Espace in Toulouse.

Markus Rippl received his Diploma in Electrical Engineering and Information Technology from Technische Universität München (TUM) in 2007. Since then, he has been a research associate with the Institute of Communications and Navigation (IKN) at the German Aerospace Center (DLR) in Oberpfaffenhofen near Munich. His areas of interest include GNSS integrity using receiver-side algorithms, next generation Receiver Autonomous Integrity Monitoring (RAIM) algorithms and architectures, and the development of a future integrity architecture supporting Advanced Receiver Autonomous Integrity Monitoring (ARAIM) with an Integrity Support Message (ISM).

ABSTRACT

This paper addresses the integration between Global Navigation Satellite System (GNSS) and Inertial Navigation System (INS) from an integrity perspective. In order to achieve this, we analyze a low-complex coupling scheme, where a GNSS layer resets the INS strapdown algorithm with position, velocity and their respective protection levels. In particular, RAIM and Velocity RAIM algorithms are used here as the integrity-based core system. Special focus is dedicated to the propagation of uncertainties in terms of covariances through the strapdown inertial algorithm, as well as the impact of the reset uncertainties and accelerometer noise on the final computed protection levels. Finally, it is shown how our integrated system may solve the continuity and availability problems of GNSS by coasting not only the position solution but also the protection levels.

1 INTRODUCTION

In civil aviation, it is considered that the probability to have a navigation error larger than a specified Alert Limit (AL) should remain below 10^{-7} or even below 10^{-9} for CAT III precision approach [1]. For stand-alone satellite navigation systems, it is a tremendous challenge to achieve these requirements due to a large variety of ranging error sources [2] and possible weak geometries that may badly affect the position accuracy.
Hence, the satellite navigation community has developed augmentation systems and integrity monitoring algorithms to guarantee the performance for a given phase of flight, e.g., Space Based Augmentation Systems (SBAS) [3], Ground Based Augmentation Systems (GBAS) [4] and Air-

borne Based Augmentation Systems (ABAS) like the Receiver Autonomous Integrity Monitoring (RAIM) [5, 3, 6, 7]. All these augmentation systems use the notion of protection levels to define position bounds at given integrity risk values. This integrity metric assumes *nominal* behavior of each ranging source provided that *abnormal* ranging errors are detected reliably, i.e., with a very low probability of missed detection.

Additionally to the integrity, a continuity requirement needs also to be fulfilled. The continuity requirement as defined for example in [1] and [3] includes: the probability to lose the navigation solution (e.g., due to radio frequency interference causing a drop in the number of visible satellites below the minimum number of four); the probability that an integrity monitor flags the GNSS solution (or a critical number of ranging sources); and the probability that the provided protection level is larger than the required alert limit during a given period of time.

In this paper, we consider the use of Inertial Reference Systems (IRS) to coast a guaranteed position solution during a loss of GNSS continuity. The idea of coasting GNSS position solution during a GNSS outage is not new and integrated system solutions can be already found on the market. Their level of accuracy achieved is fully acceptable for outages not exceeding a few minutes with navigation or tactical grade inertial units. But guaranteeing the integrity of the navigation solution during the coasting phase is very challenging and necessitate a generalization of the legacy concept of integrity.

In order to address the integrity problem, this work considers a simple integration of a GNSS and an Inertial Navigation System (INS), i.e., the stand-alone GNSS solution is taken whenever it is available with sufficient integrity, and stand-alone inertial-based navigation solution is chosen during a discontinuity of the GNSS service. The protection level of the integrated solution is defined as follows: when the GNSS service is available, we take the protection level provided by a ranging domain RAIM considering only one possible satellite outage at a time. During the coasting phase, we assume generalized inertial error models. We estimate the sensor errors propagation during the strap-down process and scale the position and velocity error bounds (protection levels) to the corresponding integrity risk quantiles.

The paper is organized as follows: We first present the GNSS-aided INS integrity concept, then in a second part we briefly recall the GNSS integrity concept including a position and velocity RAIM based protection levels. In a third part we present the strap-down INS uncertainty propagation as well as a proof of the protection levels coasting concept in a real scenario. Finally conclusion with proposed directions of a future work close this paper.

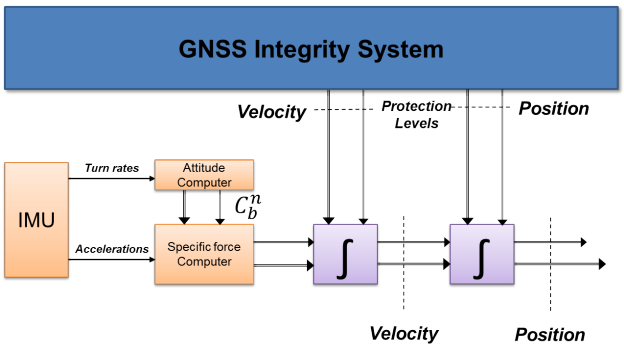

Fig. 1 GNSS-aided INS integration scheme using GNSS based position, velocity and integrity information as inertial reset.

2 GNSS-AIDED INS INTEGRITY CONCEPT

As it has been mentioned before, the overbound of the pseudoranges errors and its characterization has been widely studied for the GNSS system [8, 9, 2]. However for an integrated INS/GNSS system, the integrity problem is still an open question. In the community, a great effort has been dedicated to improve the accuracy of an integrated INS/GNSS system, i.e., many sophisticated methods and filters have been proposed and designed to enhance the system accuracy [10, 11]. However, all these algorithms are very difficult to analyze in terms of integrity due to the required linearization assumptions in inertial [12] and resulting temporal error correlations.

Similar to [13], we encounter the INS/GNSS problem from the integrity perspective. For this purpose, we choose a simple coupling scheme that enables us to assess the integrity of the whole system, even if it is not the optimal method in terms of accuracy. As seen in Fig. 1, the GNSS integrity layer not only provides a position and velocity solution as usual, but also the associated integrity information in terms of protection levels. This information is used to reset both the strapdown inertial system as well as the inertial integrity assessment. If no GNSS integrity information is available, the reset is not performed. Consequently, the reset values used in the inertial guarantee the required integrity requirements such as probability of false alarm and the integrity risk.

In order to provide the required GNSS integrity information of the position and velocity, RAIM [8] and velocity RAIM [14] are considered. In Fig. 2, the corresponding block diagram of the full system is displayed. As it can be seen, the GNSS works completely independent of the INS, i.e., there is neither feedback information to the GNSS nor in the strapdown algorithm. This allow us to analyze the nominal system error behavior in a formal way and propagate the uncertainties through the integration process.

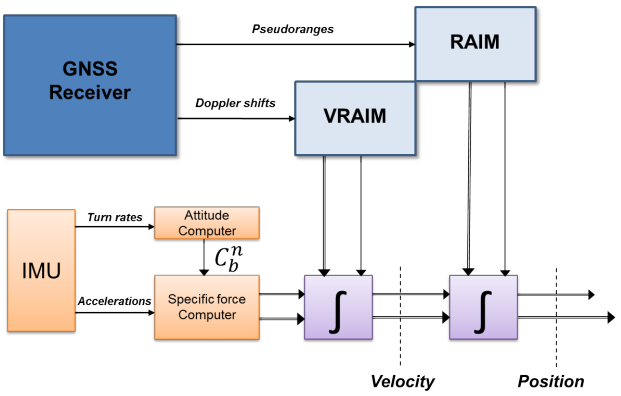

Fig. 2 GNSS-aided INS integration scheme using RAIM and velocity RAIM as GNSS integrity source.

3 GNSS INTEGRITY LAYER

In this section we discuss briefly the applied RAIM and Velocity RAIM algorithms. Additionally, we expose how the protection levels are adapted to the covariance matrix, which are used to reset the inertial system.

3.1 Receiver Autonomous Integrity Monitoring (RAIM)

RAIM is a user-level integrity scheme that has been extensively investigated as long as GNSS has been used for integrity-related applications such as guidance for aircraft. It is based on exploiting that the least-squares system of equations is over-determined. This is the case when the number of satellites is larger than the dimension of the state vector to be estimated. With more observations being present than unknown quantities to be resolved, RAIM can check the consistency of the measurements with respect to a particular solution.

In this work, we apply the weighted RAIM scheme introduced in [8]. The following section explains merely its concept; a complete derivation can be found in the original paper.

Given a weighted system of N linearized equations for the state vector $\mathbf{x}$, containing the 3D position and user clock offset estimates,

$$\mathbf{x} = \left(\mathbf{G}^T\mathbf{W}\mathbf{G}\right)^{-1}\mathbf{G}^T\mathbf{W}\rho\,, \tag{1}$$

the residuals of this least squares term can be determined with

$$\text{WSSE} = \rho^T \cdot \mathbf{W}\left(\mathbf{I} - \left(\mathbf{G}\left(\mathbf{G}^T\mathbf{W}\mathbf{G}\right)^{-1}\mathbf{G}^T\mathbf{W}\right)\right)\cdot\rho\,.$$

$\mathbf{G}$ is the design matrix containing the line-of-sight vectors, $\mathbf{W}$ is the inverse covariance-variance matrix of the measurements, $\mathbf{x}$ is the estimate of the state vector and ρ is the vector of range observations. The Weighted Sum Square Error WSSE is then a scalar test statistic that expresses the consistency of the measurement set at hand. Assuming that the measurement errors are Gaussian distributed with variances $\sigma_\mathbf{i} = \text{diag}\left(\mathbf{W}^{-1}\right)$, the distribution of the test statistic is χ^2-distributed with noncentrality parameter $\lambda = 0$ and $(N-4)$ degrees of freedom.

The consistency check on this test statistic is implemented as a hypothesis test. It employs a nominal error model for the observations to determine what degree of inconsistency is considered *nominal*. The corresponding threshold of the $WSSE$ test statistic is a function of the geometry size N and a false alert rate P_{fa}. If the fault hypothesis is chosen, the algorithm can be used for the detection of one single range failure and its exclusion. That is it tries to isolate a the faulty measurement by recursively excluding measurements until a consistent subset can be found.

Furthermore RAIM gives an estimate on the error bound given that consistency is present. From the definition of the threshold a noncentral χ^2 distribution can be established where its left tail below the threshold corresponds to the permissible missed detection rate P_{md}. For each observation the maximum error that leads to a test statistic at the level of the threshold can now be determined. Again, the nominal error model plays an important role here: It determines the test threshold for the aforementioned hypothesis test (based on the fault free hypothesis), but also relates the nominal variations of the non-faulted observations in the fault case to the distribution of the test statistic.

3.2 Velocity RAIM

The same principle used for position RAIM of fault detection and exclusion can be also applied for the computation of the velocity. GNSS receivers are able to measure the Doppler shift frequency experienced by the signal, and therefore give the information of the relative velocity (i.e., deltaranges) of every satellite in view with respect to the user. Then, combining the different deltaranges for all the satellites, it is possible to compute the velocity of the user at the same rate as the position. A deltarange ($\dot{\rho}$) can be obtained from the Doppler measurement (D) just relating it with the signal frequency (f) as $\dot{\rho} = \frac{c}{f}D$. The deltarange measurement obtained from the Doppler shift can be expressed as:

$$\dot{\rho} = \left(\mathbf{n}_u^s + \frac{\mathbf{v}^s}{c}\right)\cdot\left(\mathbf{v}^s - \mathbf{v}_u\right) - d\dot{t}^s + d\dot{t}_u + \delta + \varepsilon\,, \tag{2}$$

where $\mathbf{n}_u^s$ is the line-of-sight user-satellite vector, $\mathbf{v}^s$ and $\mathbf{v}_u$ are the satellite and user velocity respectively, $d\dot{t}^s$ and $d\dot{t}_u$ are the satellite and user clock drift, δ include the rest errors due to the atmosphere, Sagnac effect and eccentricity of the Earth and ε is the remaining noise. As in most cases the remaining noise is bigger than the other errors, δ is here considered negligible.

Combining all the measurements from the satellites in view, we end up with the following system:

$$\mathbf{\Delta}\dot{\rho} = \mathbf{G}\begin{pmatrix} \mathbf{v}_u \\ -d\dot{t}_u \end{pmatrix} - \varepsilon\,, \tag{3}$$

where $\mathbf{\Delta}\dot{\rho}$ is the measured deltarange minus the expected relative velocity given the satellite velocity and the drift of the satellite clock, and $\mathbf{G}$ is the same geometric matrix used to solve the position solution. The weighted solution of the system is computed as follows:

$$\begin{pmatrix} \mathbf{v}_u \\ -d\dot{t}_u \end{pmatrix} = \left(\mathbf{G}^T\mathbf{W}_{\Delta\dot{\rho}}\mathbf{G}\right)^{-1}\mathbf{G}^T\mathbf{W}_{\Delta\dot{\rho}}\mathbf{\Delta}\dot{\rho}\,, \tag{4}$$

where the weighted matrix $\mathbf{W}_{\Delta\dot{\rho}}$ is the inverse of the covariance of the velocity residuals. This covariance not only depends on the actual noise statistics of the deltarange measurements but also depends on the position covariance since the line-of-sight vector is needed to compute the velocity (Eq. 2). This covariance has been solved in [14] taking into account the correlation dependence with the position. Here, only the solution is shown:

$$\mathbf{W}^{-1}_{\Delta\dot{\rho}} = \mathbf{B}\mathbf{R}_{\mathbf{x}}\mathbf{B}^T + \mathbf{R}_{\dot{\rho}}\,, \tag{5}$$

where $\mathbf{R}_{\dot{\rho}}$ is the covariance of deltarange measurements, $\mathbf{R}_{\mathbf{x}}$ is the covariance of the position solution and $\mathbf{B}$ is the matrix that projects the position solution into the velocity domain through the line-of-sight vector [14].

Since the different velocity residuals can not be considered independent as in the case of the pseudoranges, the classical approach of RAIM can not be directly applied. Instead in [14], Kelly's algorithm is used to detect faults in the presence of correlated errors [15]. A fault is declared when the maximum of the N *individually normalized* residuals exceeds the threshold $T = \Phi^{-1}\left(1 - \frac{P_{\text{fa}}}{2N}\right)$ based on the probability of false alarm.

$$\text{Fault if: } T > \max_{i\in(1..N)}\left|\frac{w_i}{\sqrt{\left(\mathbf{S}\mathbf{W}^{-1}_{\Delta\dot{\rho}}\right)_{ii}}}\right|\,, \tag{6}$$

where $\mathbf{S} = \mathbf{I} - \mathbf{G}\left(\mathbf{G}^T\mathbf{W}_{\Delta\dot{\rho}}\mathbf{G}\right)^{-1}\mathbf{G}^T\mathbf{W}_{\Delta\dot{\rho}}$ projects the measurement space into the residual space and $\mathbf{w} = \mathbf{S}\Delta\dot{\rho}$ is therefore the vector of residuals.

The protection levels are computed as the sum between the minimum detectable bias projected in the velocity domain (for the worst slope) and the portion of the noise error that exceeds the integrity risk. For any direction 'x':

$$xPL = \max_i\left(\left|x_i^{\text{slope}}\right|\right)p_{\text{bias}} + K\sqrt{\sigma_x^2}\,, \tag{7}$$

where K is the inflation factor based on the integrity risk, σ_x^2 is the variance of the deltaranges projected in the 'x' direction, p_{bias} is minimum detectable bias computed as $p_{\text{bias}} = T + \Phi^{-1}(1 - P_{\text{md}})$ [15] and

$$\max_i\left(\left|x_i^{\text{slope}}\right|\right) = \max_i\left(\frac{\mathbf{H}_{xi}\sqrt{\mathbf{S}\mathbf{W}^{-1}_{\Delta\dot{\rho}}}}{|\mathbf{S}_{ii}|}\right)\,, \tag{8}$$

with $\mathbf{H} = \left(\mathbf{G}^T\mathbf{W}_{\Delta\dot{\rho}}\mathbf{G}\right)^{-1}\mathbf{G}^T\mathbf{W}_{\Delta\dot{\rho}}$.

3.3 From Protection levels to Covariances

RAIM and Velocity RAIM algorithms provide us with protection levels that satisfy the required probability of false alarm (P_{fa}) and the integrity risk (IR). However, inertial integrity uncertainty is propagated assuming Gaussian distributions through the integration process and needs therefore the uncertainty of the reset position and velocity in terms of covariance matrix. In order to adapt the protection levels (PL) computed by the GNSS algorithms to the covariances used in the inertial reset, we interpret the PL as the upper bound of a confidence interval in the three navigation directions (i.e., east-north-up). We consider therefore this protection levels as the quantiles at the integrity risk of a multivariate Gaussian distribution. Hence, we are able to build the covariance matrix with the deflated protection levels to the 1-sigma variance in every direction independently. Our GNSS covariance reset (both for velocity and position) can be computed as:

$$\mathbf{P}_{\text{GNSS}} = \begin{pmatrix} \sigma_e^2 & 0 & 0 \\ 0 & \sigma_n^2 & 0 \\ 0 & 0 & \sigma_u^2 \end{pmatrix}\,, \tag{9}$$

where, for example, for the east-west direction:

$$\sigma_e = \frac{\text{EWPL}}{\sqrt{2}\cdot\text{erf}^{-1}(1 - 2\cdot\text{IR})}\,, \tag{10}$$

where EWPL is the east-west protection level and erf^{-1} is the inverse error function. Notice that this covariance matrix is not the 1-sigma covariance of the GNSS integrity solution, nevertheless, it is the equivalent covariance that guarantee the probability of false alarm at the integrity risk of our application.

4 STRAPDOWN INS UNCERTAINTY PROPAGATION

In an Inertial Navigation System (INS), initial conditions for position and velocity must be provided so that we can coast the position of a vehicle. Here, we provide the INS with velocity and position information as well as their expected reliability in terms of protection levels at each reset. In order to determine this reliability information also during GNSS gaps, we have to understand how the given uncertainties are propagated within the inertial strapdown

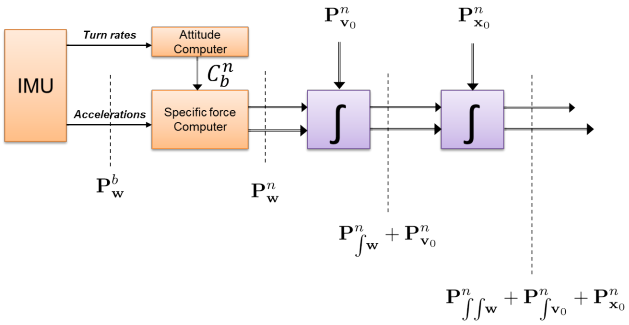

Fig. 3 Covariance propagation within the strapdown algorithm assuming given uncertainties of the velocity and position reset.

algorithm and how the error processes of the inertial measurements affect the system performance.

To analyze the strapdown inertial algorithm from the integrity point of view, we choose a simplified scenario where we consider only white noise error in the acceleration measurements with the following assumptions: the earth is considered flat and not rotating, the correction of the gravity is perfect and we have perfect information about the airplane's attitude. Under these conditions, we analyze in this section how the white noise process error in the 3D accelerations, the velocity uncertainty reset and the position reset uncertainty propagates through the algorithm. While this might seem to be a very simplified scenario, it is still very representative since in case we can overbound the rotation corrected accelerations with a Gaussian distribution, the evolution through the integration steps of the protection levels still applies as presented in this work.

The error process in the inertial accelerations, the uncertainty of the GNSS velocity reset and the uncertainty the GNSS position reset can be seen as three independent processes since they are generated by three different physical measurement methods. Hence, their associated uncertainties in terms of covariances can be integrated and propagated independently. In Fig. 3, we can see the existent covariances at every step. We define $\mathbf{P}^b_{\mathbf{w},k}$ as the 3D covariance of the white noise in the body frame, $\mathbf{P}^n_{\mathbf{w},k}$ is the covariance of the rotated accelerations (i.e., in the navigation frame), $\mathbf{P}^n_{\mathbf{v}_0,k}$ is the covariance of the velocity reset and $\mathbf{P}^n_{\mathbf{x}_0,k}$ is the covariance of the position reset. The total covariance at the velocity channel is therefore:

$$\mathbf{P}^n_{\mathbf{v},k} = \mathbf{P}^n_{\mathbf{v}_0,k} + \mathbf{P}^n_{\int w,k} \,, \tag{11}$$

where $\mathbf{P}^n_{\int w,k}$ is the covariance of single integrated white noise. And the total covariance at the position domain is expressed as:

$$\mathbf{P}^n_{\mathbf{x},k} = \mathbf{P}^n_{\mathbf{x}_0,k} + \mathbf{P}^n_{\int \mathbf{v}_0,k} + \mathbf{P}^n_{\int\int w,k} \,, \tag{12}$$

where $\mathbf{P}^n_{\int \mathbf{v}_0,k}$ is the covariance of single integrated velocity reset and $\mathbf{P}^n_{\int\int w,k}$ is the covariance of double integrated white noise.

4.1 White Noise Covariance propagation

In the following, we derive the covariance expression of the rotated first and double integrated white noise due to the acceleration errors. In [13, 16] this evolution has been addressed for a double integrated single axis. Here, we derive those expression for the generalized 3D problem and we take additionally into account the rotation of the acceleration to the navigation frame before integration.

If $\mathbf{b}_{w,k}$ is the white process noise at time k, we can express the rotation and first integration applying backwards Euler method as:

$$\mathbf{b}^n_{\int w,k} = \mathbf{b}^n_{\int w,k-1} + \Delta t \mathbf{C}^n_{b,k} \mathbf{b}_{w,k} \,, \tag{13}$$

assuming $\mathbf{b}^n_{\int w,0} = 0$. Please notice that $\mathbf{C}^n_{b,k}$ is here a deterministic rotation matrix that transforms from the body to the navigation frame (since we assume the attitude to be perfectly known) and the time interval between measurements is denoted by Δt. The latter equation can be more conveniently expressed in this summation fashion:

$$\mathbf{b}^n_{\int w,k} = \Delta t \sum_{i=1}^{k} \mathbf{C}^n_{b,i} \mathbf{b}_{w,i} \,. \tag{14}$$

We can compute then the covariance of the first integrated white noise as:

$$\begin{aligned}
\mathbf{P}^n_{\int w,k} &= E\left[\mathbf{b}^n_{\int w,k} \mathbf{b}^{n^T}_{\int w,k}\right] \\
&= E\left[\left(\Delta t \sum_{i=1}^{k} \mathbf{C}^n_{b,i} \mathbf{b}_{w,i}\right)\left(\Delta t \sum_{i'=1}^{k} \mathbf{C}^n_{b,i'} \mathbf{b}_{w,i'}\right)^T\right] \\
&= E\left[\Delta t^2 \sum_{i=1}^{k}\sum_{i'=1}^{k} \mathbf{C}^n_{b,i} \mathbf{b}_{w,i} \mathbf{b}^T_{w,i'} \mathbf{C}^{n^T}_{b,i'}\right] \,.
\end{aligned} \tag{15}$$

Since the white noise is considered independent at every time step, all the cross products between the two summation factors where $i \neq i'$ are zero, and we can rewrite:

$$\mathbf{P}^n_{\int w,k} = \Delta t^2 \sum_{i=1}^{k} \mathbf{C}^n_{b,i} \underbrace{E\left[\mathbf{b}_{w,i} \mathbf{b}^T_{w,i}\right]}_{\mathbf{Q}_{w,i}} \mathbf{C}^{n^T}_{b,i} \,. \tag{16}$$

The noise covariance $\mathbf{Q}_w$ is assumed to be a diagonal matrix since we consider the same noise power for every axis. Consequently, we can write

$$E\left[\mathbf{b}_{w,i} \mathbf{b}^T_{w,i}\right] = \mathbf{Q}_{w,i} = \sigma^2_{w,i} \mathbf{I} = \sigma^2_w \mathbf{I} \,,$$

and we can thus rewrite the covariance of the first integrated white noise as:

$$\begin{aligned}
\mathbf{P}^n_{\int w,k} &= \sigma^2_w \Delta t^2 \sum_{i=1}^{k} \mathbf{C}^n_{b,i} \mathbf{I} \mathbf{C}^{n^T}_{b,i} \\
&= \sigma^2_w \mathbf{I} \Delta t^2 \sum_{i=1}^{k} 1 \\
&= \mathbf{Q}_w \Delta t^2 k \,.
\end{aligned} \tag{17}$$

In the latter expression, since $\mathbf{C}_b^n$ is a rotation matrix, the following identity has been used:

$$\mathbf{C}_{b,i}^n \mathbf{C}_{b,i}^{n^T} = \mathbf{C}_{b,i}^n \mathbf{C}_{b,i}^{n^{-1}} = \mathbf{I}\,.$$

In the same way, we can integrate again the white process noise with an Euler formulation as:

$$\mathbf{b}_{\int\int w,k}^n = \mathbf{b}_{\int\int w,k-1}^n + \Delta t \mathbf{b}_{\int w,k}^n\,, \tag{18}$$

or in a summation expression as:

$$\begin{aligned}\mathbf{b}_{\int\int w,k}^n =& \Delta t^2 \sum_{i=1}^{k}\sum_{j=1}^{i} \mathbf{C}_{b,j}^n \mathbf{b}_{w,j} \\ =& \Delta t^2 \sum_{i=1}^{k} (k-i+1)\mathbf{C}_{b,i}^n \mathbf{b}_{w,i}\end{aligned} \tag{19}$$

with $\mathbf{b}_{\int\int w,0}^n = \mathbf{b}_{\int\int w,1}^n = 0$.

The derivation of the covariance of the rotated and double integrated white noise can be seen in Equation (20).

$$\begin{aligned}\mathbf{P}_{\int\int w,k}^n &= E\left[\mathbf{b}_{\int\int w,k}^n \mathbf{b}_{\int\int w,k}^{n^T}\right] = E\left[\left(\Delta t^2 \sum_{i=1}^{k}(k-i+1)\mathbf{C}_{b,i}^n \mathbf{b}_{w,i}\right)\left(\Delta t^2 \sum_{i'=1}^{k}(k-i'+1)\mathbf{C}_{b,i'}^n \mathbf{b}_{w,i'}\right)^T\right] \\ &= \Delta t^4 \sum_{i=1}^{k}(k-i+1)^2 \mathbf{C}_{b,i}^n E\left[\mathbf{b}_{w,i}\mathbf{b}_{w,i}^T\right]\mathbf{C}_{b,i}^{n^T} = \mathbf{Q}_w \Delta t^4 \sum_{i=1}^{k}(k-i+1)^2 = \mathbf{Q}_w \Delta t^4 \left(\frac{1}{6}k(k+1)(2k+1)\right)\,.\end{aligned} \tag{20}$$

Here, the simplification for time independence and the assumption of same noise power for all axis have been also made.

As we observe from the derived expressions, the single and the double integrated white-noise do not depend on the rotation matrices and therefore, they are independent of the movement of the sensor.

In order to validate the derived equations and covariance evolution we have run Monte-Carlo simulations using 50.000 random paths. The trajectory of the Monte-Carlo simulation is displayed in Fig. 4. Here we consider a constant altitude flight with an initial velocity of 20 m/s in north direction, the frequency of the measurements is 20 Hz and the assumed noise of the acceleration data has zero mean and $\sigma = 0.02$ m/s^2. While turning, we assumed a constant bank angle of 30 °.

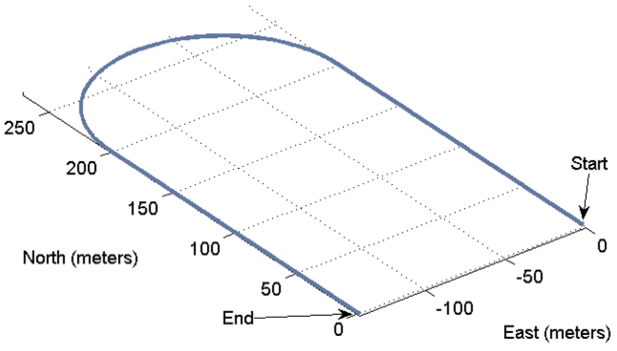

Fig. 4 Horizontal flight trajectory of the Monte-Carlo simulation.

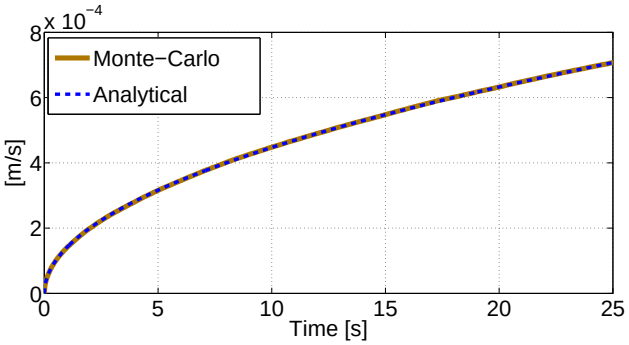

Fig. 5 Evolution of the standard deviation of the rotated and single integrated acceleration (i.e., in velocity domain) in the east direction.

The evolution of the variance in the east direction of rotated and single integrated white-noise is shown in Fig. 5. Since there is no cross correlation in the covariance matrix this is just the square root of the diagonal element. Furthermore, it coincides also with the results in the other directions.

In Fig. 6, the variance of the double integrated white noise in the east direction is also shown. We can see how the empirical variance obtained from the simulated runs matches the analytical solution.

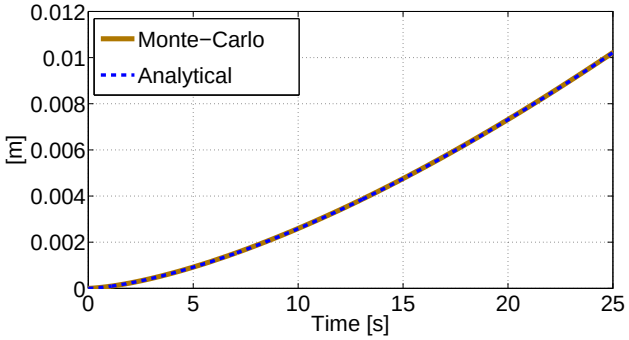

Fig. 6 Evolution of the standard deviation of the double integrated acceleration (i.e., in position domain) in the east direction.

4.2 Protection Levels Evolution

Using the derived equations of covariance propagation within the strapdown algorithm, we can determine how the corresponding protection levels are evolving in our previous presented scheme (Fig. 3). The final covariance obtained at position domain are converted to protection levels just by inflating the square root of the diagonal elements for every direction to fit the required integrity risk. Regarding the evolution of the final protection levels, three parameters has to be considered: the variance of the considered white noise in the accelerations, the protection levels of the velocity reset and the PL of the position reset. In the following, we analyze the dependency of the overall protection level based on these three parameters.

Sensitivity to White Acceleration Noise
The variance of the considered white noise is directly linked to the quality of the accelerometer. Evidently, this white noise is very critical to the system performance, since it is doubled integrated and their covariances grows quadratically. Please note that this variance assessment is also applicable in case of a Gaussian error overbound after the specific force computer (i.e., Gaussian overbound of the rotated acceleration).

In Fig. 7, we can see the evolution of the final computed protection level of one of the axis at the position domain for different considered qualities of accelerometers, i.e., for different assumed standard deviations of the white noise error process in the accelerations.

Sensitivity to Velocity Protection Level Reset
The velocity reset, since it is also integrated, has a big impact in the final protection level in the position. In Fig. 8, we can see the impact of the uncertainty of the velocity reset, where the dependency of the final position PL is plot for different velocity PL reset.

We can observe the square root shape of the curves for bigger velocity protection levels, which corresponds to the shape of a first integrated Gaussian process. For lower values of velocity PL, where the magnitude is comparable with the fixed variance of the acceleration white noise, this latter leads the increment of the final protection level. It can be also concluded that the velocity PL is a really sensitive parameter as well, since its value will have a big impact in the slope of the position PL evolution.

Sensitivity to Position Protection Level Reset
Finally, we analyze the impact of the position reset in the integrated position PL. In Fig. 9, the evolution of the PL for different position reset conditions is shown. We observed that over time, the evolution of the PL converges to an asymptotic slope regardless of the initial position PL conditions. Although, this may lead to the conclusion that the position protection level has few impact, this convergence occurs for large values of protection levels, where most probably the alert limit has been already reached.

From Fig. 7, 8 and 9 we can estimate the maximum coasting duration until the position protection level is crossing a certain alert limit, for the three critical parameters, respectively. We also gain a feeling on how sensitive the overall PL is with respect to the these values.

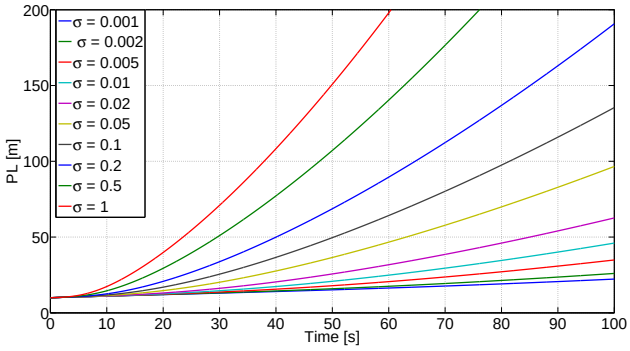

Fig. 7 Position protection level evolution for different variances of the white noise process on the acceleration. The GNSS protection levels of the rests are assumed with velocity PL reset $= 2\ m/s$ and position PL reset $= 10\ m$.

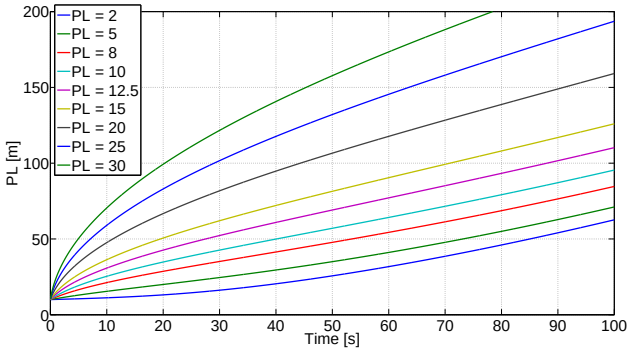

Fig. 8 Position protection level evolution for different reset protection levels in the velocity domain. Assumption: White noise variance of $\sigma = 0.02\ m/s^2$ for acceleration and a position PL reset $= 10\ m$.

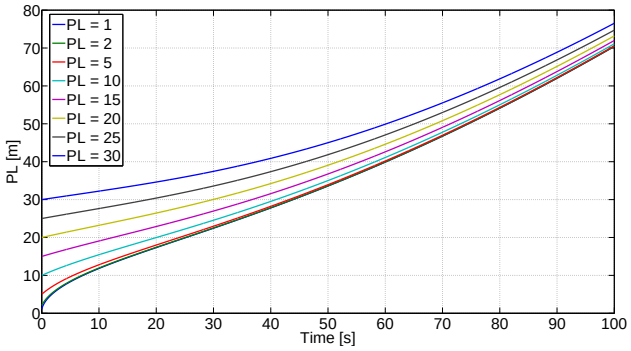

Fig. 9 Final protection level evolution for different protection level reset in the position domain. In this plot: $\sigma = 0.02\, m/s^2$, Velocity PL reset $= 2\, m/s$.

5 PROOF OF CONCEPT

In order to demonstrate our concept, we used recorded GNSS measurements from one of the DLR's measurement campaigns at our research airport in Braunschweig, Germany in 2011. The inertial measurements have been simulated so that they could satisfy the assumptions made in this work.

We focus here on one of the taxiing maneuvers. The full maneuver can be seen in Fig. 10. While the plane was taxiing from its parking position along the taxiway to the runway, the plane passed alone a nearby hangar. Therefore, some of the GPS signals were blocked and/or reflected, and cause multipath effects at the GNSS receiver. As a consequence, GNSS protection level suddenly jumped tremendously for around 100 s. This is depicted in Fig. 11. It can be seen that both east-west (EWPL) and north-south (NSPL) protection levels of standalone GPS computed with RAIM increases over 250 m. On the contrary, our GNSS-aided INS approach is able to coast not only the position solution but also the protection levels during the GPS outage.

Fig. 10 Taxiing scenario with GPS outage nearby the hangar

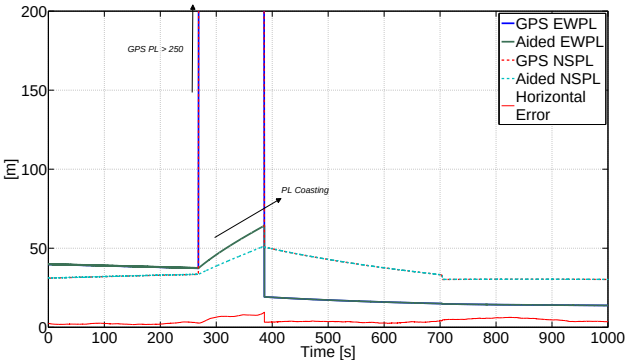

Fig. 11 Protection level coasting while taxiing during GPS outage

6 CONCLUSIONS

In this work, we have stressed the importance of addressing the GNSS/INS integration from the integrity point of view. Although it is not an easy task to perform a full analytical study of the real uncertainty propagation through the fusion algorithms, we presented here a simplified scenario where the formal propagation of covariances can be analytically solved. In particular, we focused our investigations in the strapdown integration steps and have shown the impact of the measurement noise, as well as the velocity and position reset information. Since the velocity reset has a large impact in the PL evolution, efforts should be invested to improve the velocity RAIM algorithm and to better characterize its noise level. On the other hand, the reference position reset is also essential, so further work should consider ARAIM or GBAS as the GNSS integrity layer.

The characterization of the inertial error propagation through the navigation equations presented in this work still requires some strong assumptions on the inertial measurement equipment. That is we assume the gyroscope as perfect and only consider white-noise in the accelerations. More studies of the different error processes presented on both gyroscopes and accelerometers have to be done. As this is a complex problem and no analytical solution may be derived, the solution might consist of overbounding the inertial errors after the body-to-navigation frame rotation. If performing this overbound by a Gaussian distribution, the analysis presented in this paper applies directly.

In this study, the protection levels in the horizontal plane has been considered independently, i.e., separated in East-West and North-South. This may lead to a solution where one of the protection levels is very high compared to the other. Some further attention should be drawn to the way these protection levels are compared with the corresponding alert limit, which is currently divided into horizontal and vertical only. Consequently, the system availability could be investigated in a more general manner.

REFERENCES

[1] ICAO, *Annex 10 to the Convention on International Civil Aviation: Aeronautical Telecommunications, Volume I: Radio Navigation Aids*, ICAO Std., Rev. 6th. Edition, July 2006.

[2] B. Belabbas, F. Petitprez, and A. Hornbostel, "UERE Analysis for Static Single Frequency Positioning Using Data of IGS Stations," in *ION- National Technical Meeting, San Diego- USA, January 24-26, 2005*, vol. Session A4, 2005.

[3] RTCA/SC-159, "RTCA/DO-229D Semi-Final: Minimum Operational Performance Standards for Global Positioning System/Wide Area Augmentation System Airborne Equipment," RTCA, Tech. Rep., 2006.

[4] RTCA DO-253C, " Minimum Operational Performance Standards for GPS Local Area Augmentation System Airborne Equipment," Radio Technical Commission for Aeronautics, Tech. Rep. 253C, 2008.

[5] RTCA, "Minimum Operational Performance Standards for Global Positioning System/Aircraft Base Augmentation System," SC-159, Tech. Rep. DO-316, 2009.

[6] P. Misra and P. Enge, *Global Positioning System: Signals, Measurements, and Performance*. Ganga-Jamuna Press, 2006.

[7] R. Conley, R. Cosentino, C. J. Hegarty, E. D. Kaplan, J. L. Leva, M. U. de Haag, and K. V. Dyke, *Understanding GPS, Principles and Applications*. Artech House Publishers, 2006, ch. Performance of Stand-Alone GPS, pp. 301–378.

[8] T. Walter and P. Enge, "Weighted RAIM for Precision Approach," in *Proceedins of the ION GPS*. Institute of Navigation, 1995, pp. 1995 – 2004.

[9] J. Rife, S. Pullen, B. Pervan, and P. Enge, "Paired overbounding and application to GPS augmentation," in *Position Location and Navigation Symposium, 2004. PLANS 2004*, 2004.

[10] P. D. Groves, *Principles of GNSS, Inertial, And Multisensor Integrated Navigation Systems*, 2nd ed. Artech House, 2013.

[11] Y. Yi and D. Grejner-Brzezinska, "Tightly-coupled GPS/INS Integration Using Unscented Kalman Filter and Particle Filter," in *Proceedings of the 19th International Technical Meeting of the Satellite Division of The Institute of Navigation (ION GNSS 2006)*, Fort Worth, TX, September 2006.

[12] D. Titterton and J. Weston, *Strapdown Inertial Navigation Technology, 2nd ed.* Institution of Electrical Engineers, 2004.

[13] A. Grosch and B. Belabbas, "Parameter Study of Loosely Coupled INS/GNSS Integrity Performance," in *Proceedings of IEEE/ION PLANS*, Myrtle Beach, SC, USA, 24-26 Apr 2012 2012.

[14] B. Romney, "Velocity RAIM," in *International Technical Meeting (ITM) of The Institute of Navigation*, January 2013.

[15] R. Kelly, "The linear model, rnp, and the near-optimum fault detection and exclusion algorithm." *NAVIGATION: Journal of the Institute of Navigation*, vol. V, pp. 227–259, 1998.

[16] J. H. Wall and D. M. Bevly, "Characterization of Inertial Sensor Measurements for Navigation Performance Analysis," in *ION GNSS 19th International Technical Meeting of the Satellite Division*, September 2006.